

Understanding the Quality Factor of Mass-Loaded Tensioned Resonators

R. Shaniv, S. Kumar Keshava, C. Reetz, and C. A. Regal

(Dated: September 7, 2022)

Mechanical resonators featuring large tensile stress have enabled a range of experiments in quantum optomechanics and novel sensing. Many sensing applications require functionalizing tensioned resonators by appending additional mass to them. However, this may dramatically change the resonator mode quality factor, and hence its sensitivity. In this work, we investigate the effect of the crossover from no mass load to a large mass load on the mode shape and quality factor of a tensioned resonator. We show through an analytical model and finite element analysis that as the load mass increases, surprisingly, the resonator mode shape becomes independent of the exact load mass, and therefore, its quality factor saturates. We validate this saturation effect experimentally by measuring the quality factor of a silicon nitride trampoline resonator while varying the load mass in a controlled manner.

Micromechanical and nanomechanical resonators have been a fruitful topic of research for several decades. They have shown promise for exploring quantum physics [1], in studies ranging from quantum transduction protocols [2–4], creation of quantum memories [5–7], to the generation of squeezed light [8–10], and for precision sensing applications, such as magnetic force detection [11–13], nanoscale imaging [14, 15], accelerometer design [16, 17], and mass sensing [18–20].

An adequate sensor requires both appreciable coupling to the physical parameter it is designed to sense and as low as possible environmental noise. An important figure of merit that quantifies the sensitivity of a resonator normal mode is the quality factor, denoted hereafter as Q . The Q depends on environmental isolation and is a measure of the number of coherent oscillations a resonator mode can provide before losing a significant portion of its energy to the environment [1, 21]. Therefore, resonator modes with utmost Q values are ideal for sensing.

To couple a sensor to a quantity of interest, it is often necessary to functionalize it with a coupling agent, resulting in an additional resonator mass, e.g. magnetic particles for magnetic force sensing [11, 13] or test masses for acceleration detection [16, 17]. Certain applications, such as those that aim to measure gravitational forces, require appending a mass that is much larger than the resonator mass [22–24]. In general, specific interest is devoted to modes in which the mass moves appreciably. For a large mass, typically, a single mode has a significant motion in the load, and it is usually the lowest frequency or fundamental mode. Although essential for sensing, the addition of a load mass might lower the resonator’s Q , and degrade its performance as a sensor. It is therefore of interest to understand how the Q of a resonator mode is affected by mass loading.

The Q of a resonator mode is defined as $Q = 2\pi \frac{W}{\Delta W}$, where W is the energy stored in the mode, and ΔW is the energy loss per oscillatory cycle [21]. In general, ΔW is a sum of the contributions from multiple individual loss mechanisms [25]. One way to improve the Q of a resonator is by increasing the stored energy without a

similar increase in the dissipation. This can be achieved by using a tensioned or high-stress film as the resonator and it is the result of a phenomenon called dissipation dilution [26–28]. In addition to increased Q , high-stress also extends the mode spectrum of a resonator to higher frequencies for a given resonator length scale. High frequency is of interest for certain sensing protocols, while being out of reach for similar-dimension non-tensioned sensor geometries such as cantilevers.

Low optical absorption combined with high-stress obtained in fabrication, make silicon nitride (SiN) a natural material for the design of high Q resonators [29–31]. In tensioned SiN resonators, typically, the Q of modes are limited by two loss mechanisms — bending loss, which is the energy lost due to the bending of the mode, and radiation loss, which is the energy lost from the mode via acoustic radiation into the surroundings. This allows us to define individual quality factors, Q_{bend} and Q_{rad} , which are associated with bending loss and radiation loss respectively. Therefore, we can write that $\frac{1}{Q} = \frac{1}{Q_{\text{bend}}} + \frac{1}{Q_{\text{rad}}}$. Q_{bend} can be significantly improved by tailoring the mode-shape to reduce bending loss at the mode edge, commonly referred to as clamping loss [27, 28, 32–37]. Q_{rad} can be improved by resonator patterning, substrate engineering, and strategic device mounting [27, 32, 37–44]. These techniques have led to resonators with modes limited by Q_{bend} .

In this work, we study the effect of a localized mass load on the Q_{bend} of highly tensioned resonators. We show through analytical calculations and finite element analysis (FEA) simulations that as the load mass increases, the modes of the resonator change in frequency and displacement shape. Further, we show that for a large enough mass, each mode displacement function becomes independent of the mass, which we claim leads to mass-independent Q_{bend} . We refer to this phenomenon as Q mass saturation. We validate this saturation experimentally by measuring the Q of a tensioned SiN trampoline resonator [34, 36] as a function of the load mass. We use magnetic grains for the load mass, and we vary the mass by sequentially stacking the grains using their

mutual magnetic attraction to avoid varying the amount of lossy adhesive as mass was added. This allows us to compare Q measurements for different load masses on a single device.

In order to obtain an expression for the Q_{bend} of a mode, we assume pure out-of-plane mode displacement $u(x, y)$, where x and y are in-plane resonator coordinates, as well as small displacement, $|u(x, y)| \ll h$, where h is the resonator thickness. In addition, we assume large in-plane tensile stress σ_0 , such that the speed of sound along the resonator is approximately proportional to $\sqrt{\sigma_0}$.

Then we can write $W \approx \int_V \frac{\sigma_0}{2} \left[\left(\frac{\partial u}{\partial x} \right)^2 + \left(\frac{\partial u}{\partial y} \right)^2 \right] dV$ and

$\Delta W_{\text{bend}} \approx \int_V \frac{\pi E_2}{(1-\nu^2)} z^2 \left[\frac{\partial^2 u}{\partial x^2} + \frac{\partial^2 u}{\partial y^2} \right]^2 dV$, where E_2 is the imaginary part of the Young modulus, ν is the Poisson ratio, z is the resonator coordinate along its thickness and V is the volume of the resonator [27, 45]. This leads to:

$$Q_{\text{bend}}(u) = \frac{\int_V \sigma_0 \left[\left(\frac{\partial u}{\partial x} \right)^2 + \left(\frac{\partial u}{\partial y} \right)^2 \right] dV}{\int_V \frac{E_2}{(1-\nu^2)} z^2 \left[\frac{\partial^2 u}{\partial x^2} + \frac{\partial^2 u}{\partial y^2} \right]^2 dV} \quad (1)$$

Eq. 1 affirms that if the mode displacement function $u(x, y)$ stops changing, then Q_{bend} saturates.

We can elucidate this Q saturation and its origin through an example model. We study the fundamental mode of a highly pre-tensioned suspended beam, which is referred to as a string. (A second example for a tensioned, mass loaded circular membrane can be found in the supplementary material.) The string resonator is fixed at both ends, with displacement $u(x)$ in the vertical axis, where x is the coordinate along the resonator (Fig. 1a). Here $u(x)$ satisfies the string equation [25]:

$$\frac{Eh^2}{12\sigma_0} \frac{d^4 u}{dx^4} - \frac{d^2 u}{dx^2} - \frac{\rho(x)(2\pi f)^2}{\sigma_0} u = 0, \quad (2)$$

for $0 \leq x \leq L$, where L is the string length. Here, E , h , σ_0 , are the string's Young modulus, thickness and the tensile stress respectively, and f is the mode frequency. The string width w is absent from the equation because the string has a uniform width. The position-dependent density $\rho(x)$ accounts for possible increased density at some region $a \leq x \leq b$, for $0 < a < b < L$. We denote the density at $0 \leq x < a$ and $b < x \leq L$, subsequently referred to as the outer regions, by ρ_m , and the density at $a \leq x \leq b$, the inner region, by $\rho_m + \rho_M$, such that ρ_M is the added load density. The pre-stress σ_0 is assumed to be large, satisfying the length scale inequality $l = 2\pi \sqrt{\frac{Eh^2}{12\sigma_0}} \ll L$.

Given this high pre-stress condition the frequency of the string's fundamental mode can be well approximated by neglecting the fourth derivative term in Eq. 2 [25].

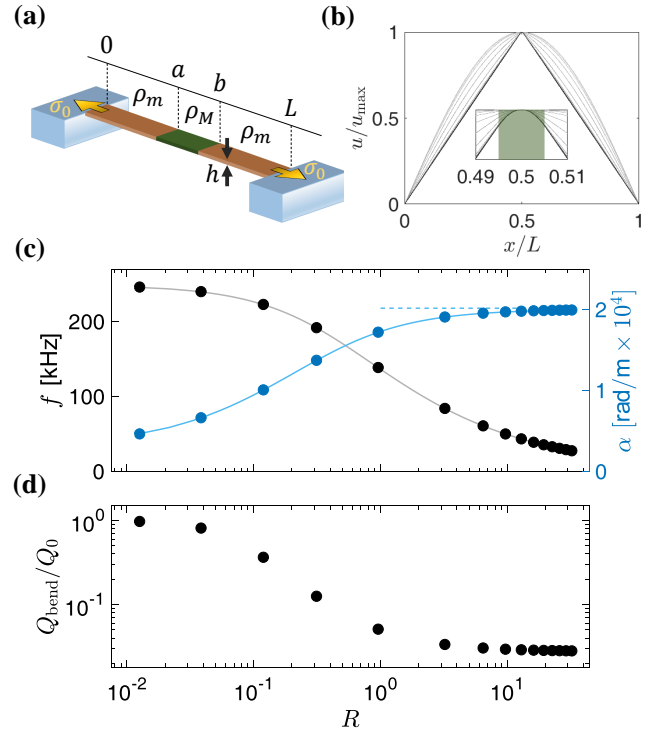


FIG. 1. **Mass loaded string theoretical model.**

(a) String parameters: A string of length L , thickness h , with tensile stress σ_0 is fixed at points $x = 0$ and $x = L$, where x is the coordinate along the length of the string, and has linear density ρ_m everywhere except for the region $a \leq x \leq b$, where the density is $\rho_M + \rho_m$. (b) Mode shape visualization: FEA simulations show the mass loaded string fundamental mode displacement normalized to its maximum displacement (lighter color corresponds to lighter mass load) plotted against the spatial coordinate normalized to the string length. The inset shows a zoomed image of the mode shape around the mass loaded region (shaded green). (c) String frequency and inner region wavenumber: FEA simulated (solid circles) and analytically calculated (solid lines) fundamental mode frequency (black) and inner region wavenumber (blue) of a string are shown as a function of R , the ratio between the mass of the load and the total mass of the unloaded resonator. FEA simulation points correspond to the different mode shapes in sub-figure (b). The analytically calculated large mass limit inner region wavenumber α_{lim} is indicated (dashed blue line). (d) String quality factor: The plot shows the fundamental mode Q_{bend} normalized to Q_0 , the Q_{bend} of an unloaded resonator, as a function of the mass ratio R . For this plot, to focus on the effect of the mass load, Q_{bend} was calculated without the mechanical clamping loss contribution from the edges of the mode. Subfigures (c) and (d) share the same horizontal coordinate, and results shown correspond to specific choice of parameters (supplementary material).

The solution then reads:

$$u(x) = \begin{cases} A_1 \sin\left(\frac{\alpha}{\sqrt{1+\chi}}x\right) & 0 \leq x \leq a \\ A_2 \sin(\alpha x) + B_2 \cos(\alpha x) & a \leq x \leq b, \\ A_3 \sin\left(\frac{\alpha}{\sqrt{1+\chi}}(L-x)\right) & b \leq x \leq L \end{cases} \quad (3)$$

where we introduced the density ratio $\chi = \frac{\rho_M}{\rho_m}$ and the inner region wavenumber $\alpha = 2\pi f \sqrt{\frac{\rho_m + \rho_M}{\sigma_0}}$, and imposed the fixed boundary conditions $u(0) = u(L) = 0$. An equation for α can be found by using the continuity of $u(x)$ and its first derivative at $x = a$ and $x = b$ (supplementary material). We see excellent agreement between FEA simulations of α and f for the fundamental mode of a string, and the corresponding numerically-evaluated analytical calculation, for different values of R the resonator mass ratio (Fig. 1c). We define the resonator mass ratio as $R = \frac{M_{\text{load}}}{M_{\text{unloaded}}}$ using the quantities $M_{\text{load}} = hw(b-a)(\rho_M)$ and $M_{\text{unloaded}} = hwL\rho_m$ corresponding to the load mass and the total unloaded resonator mass, respectively. This parameter was chosen to emphasize that we are investigating the crossover between no load ($R = 0$) and a load that is significantly more massive than the entire resonator mass ($R \gg 1$).

In addition to α and f , we used the results from the FEA simulations for the fundamental mode along with Eq. 1 to calculate Q_{bend} . Fig. 1d shows the dimensionless geometric parameter Q_{bend}/Q_0 , where Q_0 is the Q_{bend} without a load mass, as a function of R . While calculating Q_{bend} , in order to focus specifically on the effect of the load mass, we chose to exclude the mechanical clamping loss contribution from the edges of the mode. From the plot, we see that Q_{bend}/Q_0 becomes independent of the exact load mass for $R \gg 1$ and it saturates to a value that is lower than when R is close to zero. (Note the plot points corresponding to $R = 0$ have been omitted from Fig. 1c and Fig. 1d because the horizontal axis is on a logarithmic scale.)

Fig. 1b evinces that the fundamental mode inner region wavenumber α saturates to a finite value, α_{lim} , as the mass grows larger (supplementary material). Simultaneously, the outer region wavenumber diminishes, and in the large mass limit the mass loaded string equation can be approximated as

$$\frac{l^2}{(2\pi)^2} \frac{d^4 u}{dx^4} - \frac{d^2 u}{dx^2} - K^2(x) u = 0, \quad (4)$$

where

$$K^2(x) \approx \begin{cases} 0 & 0 \leq x < a, \quad b < x \leq L \\ \alpha_{\text{lim}}^2 & a \leq x \leq b \end{cases} \quad (5)$$

Because this equation is independent of the load mass, so is its solution (supplementary material).

In the high mass load limit, the mode shape of the unloaded regions can be understood in two equivalent ways. The first is temporal: for an unloaded resonator, the fundamental mode period is given by $\sqrt{\frac{\rho_m}{\sigma_0}} 2L$, which can be interpreted as the time it takes an out-of-plane mechanical perturbation to make a roundtrip across the length L of the resonator, with speed of sound $\sqrt{\frac{\sigma_0}{\rho_m}}$. As the density of the loaded region increases to the high mass load limit ($\rho_m \rightarrow \rho_m + \rho_M$) the period of the fundamental mode increases, meaning T_{loaded} is now much longer than the roundtrip time a mechanical perturbation propagates in the unloaded region. As a result, the mode shape in the unloaded regime approximates a quasi-static displacement, with the mode shape limit being a static displacement at any moment. The second is spatial: the mode wavelength $T_{\text{loaded}} \sqrt{\frac{\sigma_0}{\rho_m}}$ is much longer than the unloaded region length scale. As a result, the mode shape converges to a displacement function that doesn't curve in the unloaded region. For a string, the resulting mode shape limit is linear at the outer region, and since the inner region has to match with the outer regions at the boundaries, it implies that both the outer and inner regions approach a limit shape, which approximates a triangular shape. (Fig. 1b). This leads to the splitting of the string equation as is described in Eq. 4 and Eq. 5, and as explained, its solution is independent of the load mass which leads to Q saturation.

Although our analysis thus far has focused on the case of the mass loaded string, the key points of the explanation above apply more generally to highly tensioned mass loaded resonators of arbitrary geometry and imply Q saturation for a high enough mass load. Specifically, as an example we have also carried out an analysis for a circular membrane (supplementary material).

To validate the model-predicted Q saturation effect experimentally, we measured the fundamental mode Q , denoted hereafter as Q_{fund} , of a high-stress SiN trampoline resonator for different load masses [34, 36]. A trampoline resonator features a wide pad for low-imprecision optical detection and the geometry is designed to reduce mechanical clamping losses, allowing access to high Q modes [34, 36]. The device we used was microfabricated with 110 nm thick SiN with a side length of 1 mm, a tether width of 5 μm , and a pad area of approximately 86 μm^2 (Fig. 2b). Stoichiometric SiN with a film pre-patterning tensile stress of roughly 1 GPa was used and an unloaded fundamental mode frequency of ≈ 143 kHz was measured. The resonator was suspended from a 385 μm thick square silicon chip with a side length of 4 mm (supplementary material).

In order to vary the load mass while keeping the other variables constant, we employed a ‘‘magnetic stacking’’ technique. We used magnetic particles (Neo Magnequench MQFP-B+ (D50=25m)) as the load mass. The first par-

ticle was affixed to our device using ultra-violet (UV) cured epoxy (NEA 123SHGA) and is shown in Fig. 2a. We then magnetized the first particle by placing the device inside a strong magnetic field. Next, a second particle was brought near the first, causing the first particle's magnetic field to induce a magnetic moment in the second particle, resulting in magnetic attraction between the particles. The device was then put under a strong magnetic field once again, this time to magnetize the second particle, and effectively make both particles a single, inseparable mass load without using additional epoxy. This procedure was repeated for multiple magnetic particles (Fig. 2c) and Q_{fund} was measured between each addition of mass. Although we expect the epoxy to have high mechanical loss compared to SiN, by keeping its volume and three dimensional orientation constant through magnetic stacking, we were able to study how Q_{fund} is affected by mass loading in a systematic fashion, avoiding errors arising from multiple epoxy applications on separate devices.

We note that the Q_{fund} of trampoline resonators is sensitive to mounting due to radiation loss [34, 36]. To minimize changes in Q_{fund} due to varying radiation loss, we kept the mounting the same between Q_{fund} measurements. This was achieved by affixing our devices at one corner onto a custom-made silicon base by using silver epoxy (EPO-TEK H20E). We found that this mounting scheme consistently allowed for $Q_{\text{fund}} \approx 33 \times 10^6$ without a mass load. This matches the bending loss limited Q_{fund} obtained from FEA simulations (supplementary material), thus implying $Q_{\text{rad}} \gg Q_{\text{bend}}$, and therefore, $Q_{\text{fund}} \approx Q_{\text{bend}}$ for trampoline resonators without mass loading when mounted in this way.

The key results of our experiment are shown in Fig. 3a along with relevant FEA simulations. The open black circle and solid black circles correspond to the experimentally measured Q_{fund} values for a trampoline resonator at 300 K, without a load mass and with a variable load mass, respectively. They depict how Q_{fund} decreases as the load mass increases, but becomes distinctively insensitive at higher load mass values. This is manifested as a plateau for masses larger than ~ 10 ng and is indicative of Q saturation. The plateau value amounts to approximately four orders of magnitude reduction in Q_{fund} compared to the unloaded case. To model these results, we used FEA simulations at 300 K which took into account bending loss in both the SiN and the epoxy, while disregarding radiation loss (black dotted line). In the simulations, we scanned the epoxy length scale and loss tangent, and we chose realistic model parameters to align with our data while also setting an upper bound on Q_{fund} (supplementary material). We see reasonable agreement between our measured data and simulations. However, the simulated model does not fit all the data points to within the measurement noise, which we believe is because, irrespective of device mounting, at higher mass, and therefore lower frequency, the resonator is more susceptible to residual

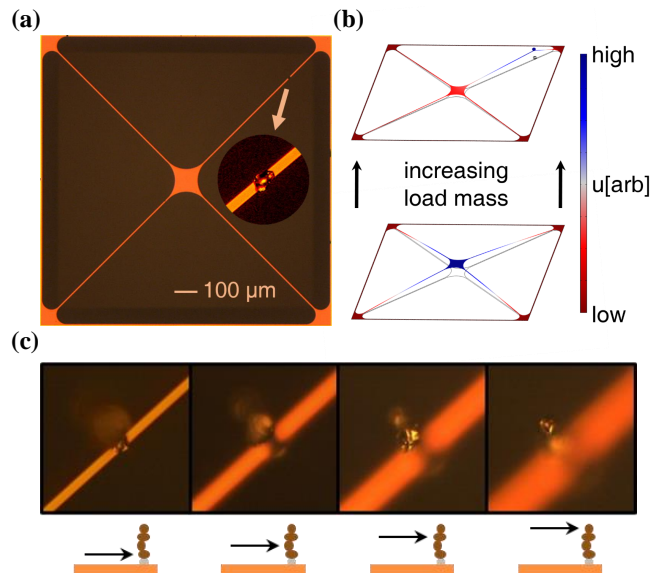


FIG. 2. **System for experimental validation.**

(a) Microscope image of device: Optical microscope image shows the trampoline resonator with a magnet deposited on its tether. The inset shows a zoomed image of the magnet. (b) Mode shape visualization: FEA simulations show the trampoline fundamental mode shape with both a high mass load (top) and without a mass load (bottom). (c) Magnetic stacking: Microscope images in different planes show a stack of four magnets, going all the way from the first magnet in focus (leftmost image) to the fourth magnet in focus (rightmost image). The drawing at the bottom shows a side-view of the trampoline resonator (orange slab) with a droplet of epoxy (grey blob) and a stack of magnets (dark brown blobs). Each drawing indicates the magnet which is in focus in the corresponding microscope image (black arrow pointing at dark brown blob).

radiation loss.

In order to further validate that the large reduction in Q_{fund} originates mainly from loss in the epoxy, rather than residual radiation loss which manifests when the load mass is large, we performed additional measurements at temperatures of 300 K and also 8 K (light pink and sky blue markers respectively), on two different devices (triangle and square). Each device was measured at both temperatures. The results show that the Q_{fund} rises by about two orders of magnitude as the resonator is cooled to cryogenic temperatures. Although SiN resonators are expected to have reduced bending loss at 8 K compared to 300 K, empirically it is by a small factor of ~ 3 , which cannot explain the measured difference in Q_{fund} [32]. We therefore conclude that when cold, the epoxy's bending loss reduces significantly, which affirms that the reduction in Q_{fund} seen is primarily due to the lossy epoxy.

A fourth device (sky blue diamond) measured at 8 K provides evidence that a fairly high quality factor $Q_{\text{fund}} \approx 3.7 \times 10^5$ can be achieved far in the saturated

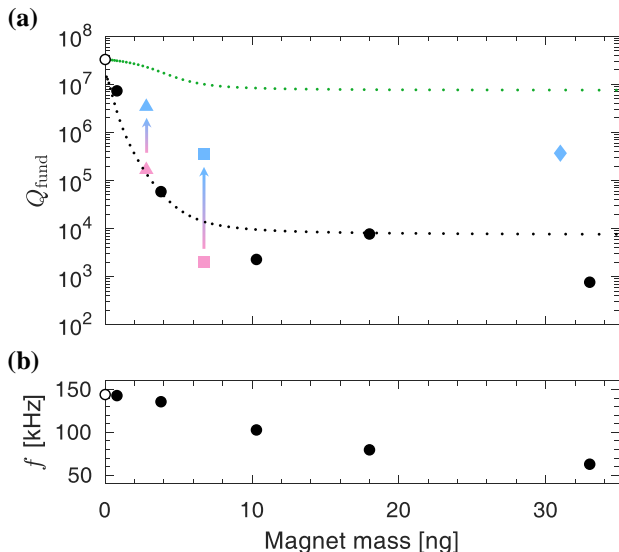


FIG. 3. **Experimental results and FEA simulations.**

(a) Trampoline Q_{fund} as a function of magnet mass: Experimentally measured Q_{fund} values at 300 K (circles) are shown without a load mass (open black circle), and with a varying load mass (solid black circles). Corresponding FEA simulated Q_{fund} results at 300 K are shown when bending loss in the epoxy is disregarded (green dotted line), and when bending loss in the epoxy is accounted for (black dotted line). Experimentally measured Q_{fund} values for two other devices (triangle and square) are shown at both 300 K (light pink) and 8 K (sky blue). The first device (triangle) has mass load of 2.8 ng and the second device (square) has mass load of 6.7 ng. Experimentally measured Q_{fund} for a third device (diamond) at 8 K (sky blue) with a large load mass of 31.0 ng is also shown. (b) Trampoline fundamental mode frequency as a function of magnet mass: Experimental frequency measurements at 300 K (circles) are shown without a load mass (open black circle) and with a varying load mass (solid black circles). Subfigures (a) and (b) share the same horizontal coordinate.

regime. Previous studies have shown that using better epoxy can lead to higher quality factors [46].

In order to set a theoretical limit on the saturated Q_{fund} at 300 K, we performed FEA simulations which only consider bending loss in the SiN and disregard all other forms of loss (green dotted line). The results indicate it is possible to obtain a Q_{fund} decrease of only a factor of ~ 1.5 (Q as high as 10^7) in the limit of a large load mass. The saturated Q_{fund} for trampolines can be further optimized by changing the location of local mass loading (supplementary material), and possibly by using trampoline resonators with carefully engineered geometries [34, 36, 47].

In conclusion, we have analyzed the problem of tensioned mechanical resonators with a local mass load. We have shown that the added mass changes the shape of the resonator fundamental mode, and therefore, the Q_{fund} of

the resonator. Further, we have demonstrated that for a large load mass, the mode shape becomes independent of the load mass and converges to a limit shape. This implies that Q_{fund} saturates in the limit of a large mass load. We have validated our model by measuring the Q_{fund} of a SiN trampoline resonator for different load masses. We believe that this work provides important guiding principles for the design of sensors where mass loading is needed, such as in magnetic field sensors [11–13], accelerometers [16, 17], mass balances [18–20], and gravity detectors [22–24, 48]. Further, the ideas presented could be extended to other high Q tensioned two dimensional devices such as phononic crystals [27, 32, 38], hierarchical structures [35, 49], and machine-learning optimized resonators [47, 50].

Acknowledgements: We thank M. Urmey for helpful comments on the manuscript. This work was supported by funding from NSF Grant No. PHYS 1734006, Cottrell FRED Award from the Research Corporation for Science Advancement under grant 27321, and the Baur-SPIE Endowed Professor at JILA.

-
- [1] M. Aspelmeyer, T. J. Kippenberg, and F. Marquardt, Cavity optomechanics, *Reviews of Modern Physics* **86**, 1391 (2014).
 - [2] R. W. Andrews, R. W. Peterson, T. P. Purdy, K. Cicak, R. W. Simmonds, C. A. Regal, and K. W. Lehnert, Bidirectional and efficient conversion between microwave and optical light, *Nature Physics* **10**, 321 (2014).
 - [3] M. Forsch, R. Stockill, A. Wallucks, I. Marinković, C. Gärtner, R. A. Norte, F. van Otten, A. Fiore, K. Srinivasan, and S. Gröblacher, Microwave-to-optics conversion using a mechanical oscillator in its quantum ground state, *Nature Physics* **16**, 69 (2020).
 - [4] M. Mirhosseini, A. Sipahigil, M. Kalaei, and O. Painter, Superconducting qubit to optical photon transduction, *Nature* **588**, 599 (2020).
 - [5] A. Wallucks, I. Marinković, B. Hensen, R. Stockill, and S. Gröblacher, A quantum memory at telecom wavelengths, *Nature Physics* **16**, 772 (2020).
 - [6] P. Kharel, Y. Chu, M. Power, W. H. Renninger, R. J. Schoelkopf, and P. T. Rakich, Ultra-high-Q phononic resonators on-chip at cryogenic temperatures, *Apl Photonics* **3**, 066101 (2018).
 - [7] G. S. MacCabe, H. Ren, J. Luo, J. D. Cohen, H. Zhou, A. Sipahigil, M. Mirhosseini, and O. Painter, Nano-acoustic resonator with ultralong phonon lifetime, *Science* **370**, 840 (2020).
 - [8] T. P. Purdy, P.-L. Yu, R. W. Peterson, N. S. Kampel, and C. A. Regal, Strong optomechanical squeezing of light, *Physical Review X* **3**, 031012 (2013).
 - [9] A. H. Safavi-Naeini, S. Gröblacher, J. T. Hill, J. Chan, M. Aspelmeyer, and O. Painter, Squeezed light from a silicon micromechanical resonator, *Nature* **500**, 185 (2013).
 - [10] D. W. Brooks, T. Botter, S. Schreppler, T. P. Purdy, N. Brahm, and D. M. Stamper-Kurn, Non-classical light generated by quantum-noise-driven cavity optomechan-

- ics, *Nature* **488**, 476 (2012).
- [11] D. Rugar, R. Budakian, H. Mamin, and B. Chui, Single spin detection by magnetic resonance force microscopy, *Nature* **430**, 329 (2004).
- [12] N. Scozzaro, W. Ruchotzke, A. Belding, J. Cardellino, E. C. Blomberg, B. A. McCullian, V. P. Bhallamudi, D. V. Pelekhov, and P. C. Hammel, Magnetic resonance force detection using a membrane resonator, *Journal of Magnetic Resonance* **271**, 15 (2016).
- [13] R. Fischer, D. P. McNally, C. Reetz, G. G. Assumpcao, T. Knief, Y. Lin, and C. A. Regal, Spin detection with a micromechanical trampoline: towards magnetic resonance microscopy harnessing cavity optomechanics, *New Journal of Physics* **21**, 043049 (2019).
- [14] C. Degen, M. Poggio, H. Mamin, C. Rettner, and D. Rugar, Nanoscale magnetic resonance imaging, *Proceedings of the National Academy of Sciences* **106**, 1313 (2009).
- [15] D. Halg *et al.*, Membrane-based scanning force microscopy, *Physical Review Applied* **15**, L021001 (2021).
- [16] A. G. Krause, M. Winger, T. D. Blasius, Q. Lin, and O. Painter, A high-resolution microchip optomechanical accelerometer, *Nature Photonics* **6**, 768 (2012).
- [17] F. Zhou, Y. Bao, R. Madugani, D. A. Long, J. J. Gorman, and T. W. LeBrun, Broadband thermomechanically limited sensing with an optomechanical accelerometer, *Optica* **8**, 350 (2021).
- [18] Y.-T. Yang, C. Callegari, X. Feng, K. L. Ekinci, and M. L. Roukes, Zeptogram-scale nanomechanical mass sensing, *Nano Letters* **6**, 583 (2006).
- [19] K. Ekinci, X. Huang, and M. Roukes, Ultrasensitive nanoelectromechanical mass detection, *Applied Physics Letters* **84**, 4469 (2004).
- [20] N. V. Lavrik and P. G. Datskos, Femtogram mass detection using photothermally actuated nanomechanical resonators, *Applied physics letters* **82**, 2697 (2003).
- [21] J. R. Taylor, *Classical Mechanics*. 3 “E ed.
- [22] Y. Liu, J. Mummery, J. Zhou, and M. A. Sillanpaa, Gravitational forces between nonclassical mechanical oscillators, *Physical Review Applied* **15**, 034004 (2021).
- [23] J. Schmole, M. Dragosits, H. Hepach, and M. Aspelmeyer, A micromechanical proof-of-principle experiment for measuring the gravitational force of milligram masses, *Classical and Quantum Gravity* **33**, 125031 (2016).
- [24] J. R. Pratt, A. R. Agrawal, C. A. Condos, C. M. Pluchar, S. Schlamminger, and D. J. Wilson, Nanoscale torsional dissipation dilution for quantum experiments and precision measurement, *arXiv preprint arXiv:2112.08350* (2021).
- [25] S. Schmid, L. G. Villanueva, and M. L. Roukes, *Fundamentals of nanomechanical resonators* (Springer, Berlin, 2016), Vol. 49.
- [26] S. A. Fedorov, N. J. Engelsen, A. H. Ghadimi, M. J. Breyhi, R. Schilling, D. J. Wilson, and T. J. Kippenberg, Generalized dissipation dilution in strained mechanical resonators, *Physical Review B* **99**, 054107 (2019).
- [27] Y. Tsaturyan, A. Barg, E. S. Polzik, and A. Schliesser, Ultracoherent nanomechanical resonators via soft clamping and dissipation dilution, *Nature Nanotechnology* **12**, 776 (2017).
- [28] A. H. Ghadimi, S. A. Fedorov, N. J. Engelsen, M. J. Breyhi, R. Schilling, D. J. Wilson, and T. J. Kippenberg, Elastic strain engineering for ultralow mechanical dissipation, *Science* **360**, 764 (2018).
- [29] B. Zwickl, W. Shanks, A. Jayich, C. Yang, A. Bleszynski Jayich, J. Thompson, and J. Harris, High quality mechanical and optical properties of commercial silicon nitride membranes, *Applied Physics Letters* **92**, 103125 (2008).
- [30] M. Yuan, M. A. Cohen, and G. A. Steele, Silicon nitride membrane resonators at millikelvin temperatures with quality factors exceeding 108, *Applied Physics Letters* **107**, 263501 (2015).
- [31] E. Serra *et al.*, Microfabrication of large-area circular high-stress silicon nitride membranes for optomechanical applications, *AIP Advances* **6**, 065004 (2016).
- [32] C. Reetz, R. Fischer, G. G. Assumpcao, D. P. McNally, P. S. Burns, J. C. Sankey, and C. A. Regal, Analysis of membrane phononic crystals with wide band gaps and low-mass defects, *Physical Review Applied* **12**, 044027 (2019).
- [33] M. J. Breyhi, A. Beccari, S. A. Fedorov, A. H. Ghadimi, R. Schilling, D. J. Wilson, N. J. Engelsen, and T. J. Kippenberg, Clamp-tapering increases the quality factor of stressed nanobeams, *Nano Letters* **19**, 2329 (2019).
- [34] C. Reinhardt, T. Muller, A. Bourassa, and J. C. Sankey, Ultralow-noise SiN trampoline resonators for sensing and optomechanics, *Physical Review X* **6**, 021001 (2016).
- [35] S. A. Fedorov, A. Beccari, N. J. Engelsen, and T. J. Kippenberg, Fractal-like mechanical resonators with a soft-clamped fundamental mode, *Physical Review Letters* **124**, 025502 (2020).
- [36] R. A. Norte, J. P. Moura, and S. Groblacher, Mechanical resonators for quantum optomechanics experiments at room temperature, *Physical Review Letters* **116**, 147202 (2016).
- [37] A. H. Ghadimi, D. J. Wilson, and T. J. Kippenberg, Radiation and internal loss engineering of high-stress silicon nitride nanobeams, *Nano Letters* **17**, 3501 (2017).
- [38] P.-L. Yu, K. Cicak, N. Kampel, Y. Tsaturyan, T. Purdy, R. Simmonds, and C. Regal, A phononic bandgap shield for high-Q membrane microresonators, *Applied Physics Letters* **104**, 023510 (2014).
- [39] M. J. Weaver, B. Pepper, F. Luna, F. M. Buters, H. J. Eerkens, G. Welker, B. Perock, K. Heeck, S. de Man, and D. Bouwmeester, Nested trampoline resonators for optomechanics, *Applied Physics Letters* **108**, 033501 (2016).
- [40] R. A. Norte, Nanofabrication for On-Chip Optical Levitation, Atom-Trapping, and Superconducting Quantum Circuits, *PhD Thesis* (2015).
- [41] D. J. Wilson, Cavity Optomechanics with High-Stress Silicon Nitride Films, *PhD Thesis* (2012).
- [42] C. Reinhardt, Ultralow-Noise Silicon Nitride Trampoline Resonators for Sensing and Optomechanics, *PhD Thesis* (2017).
- [43] A. Borrielli *et al.*, Control of recoil losses in nanomechanical SiN membrane resonators, *Physical Review B* **94**, 121403 (2016).
- [44] Z. Li, Q. Zhang, X. You, Y. Li, and K. Peng, Suppression of phonon tunneling losses by microfiber strings for high-Q membrane microresonators, *Applied Physics Letters* **109**, 191903 (2016).
- [45] P.-L. Yu, T. Purdy, and C. Regal, Control of material damping in high-Q membrane microresonators, *Physical Review Letters* **108**, 083603 (2012).
- [46] S. Schediwy, S. Gras, L. Ju, and D. Blair, High Q factor bonding using natural resin for reduced thermal noise of test masses, *Review of scientific instruments* **76**, 026117

- (2005).
- [47] D. Høj, F. Wang, W. Gao, U. B. Hoff, O. Sigmund, and U. L. Andersen, Ultra-coherent nanomechanical resonators based on inverse design, *Nature Communications* **12**, 1 (2021).
- [48] G. I. González and P. R. Saulson, Brownian motion of a mass suspended by an anelastic wire, *The Journal of the Acoustical Society of America* **96**, 207 (1994).
- [49] M. J. Breyhi, A. Beccari, R. Groth, S. A. Fedorov, A. Arabmoheghi, T. J. Kippenberg, and N. J. Engelsen, Hierarchical tensile structures with ultralow mechanical dissipation, *Nature Communications* **13**, 1 (2022).
- [50] D. Shin, A. Cupertino, M. H. de Jong, P. G. Steeneken, M. A. Bessa, and R. A. Norte, Spiderweb nanomechanical resonators via bayesian optimization: inspired by nature and guided by machine learning, *Advanced Materials* **34**, 2106248 (2022).